© 2021. Published by The Company of Biologists Ltd | Development (2021) 148, dev199578. doi:10.1242/dev.199578

RESEARCH ARTICLE

The RNA helicase Ddx52 functions as a growth switch in juvenile zebrafish

Tzu-Lun Tseng[1], Ying-Ting Wang[1], Chang-Yu Tsao[1], Yi-Teng Ke[1], Yi-Ching Lee[1], Hwei-Jan Hsu[1], Kenneth D. Poss[2] and Chen-Hui Chen[1,*]

ABSTRACT

Vertebrate animals usually display robust growth trajectories during juvenile stages, and reversible suspension of this growth momentum by a single genetic determinant has not been reported. Here, we report a single genetic factor that is essential for juvenile growth in zebrafish. Using a forward genetic screen, we recovered a temperature-sensitive allele, *pan* (after Peter Pan), that suspends whole-organism growth at juvenile stages. Remarkably, even after growth is halted for a full 8-week period, *pan* mutants are able to resume a robust growth trajectory after release from the restrictive temperature, eventually growing into fertile adults without apparent adverse phenotypes. Positional cloning and complementation assays revealed that *pan* encodes a probable ATP-dependent RNA helicase (DEAD-Box Helicase 52; *ddx52*) that maintains the level of 47S precursor ribosomal RNA. Furthermore, genetic silencing of *ddx52* and pharmacological inhibition of bulk RNA transcription similarly suspend the growth of flies, zebrafish and mice. Our findings reveal evidence that safe, reversible pauses of juvenile growth can be mediated by targeting the activity of a single gene, and that its pausing mechanism has high evolutionary conservation.

KEY WORDS: Zebrafish, Forward genetics, Regeneration, RNA helicase, *ddx52*

INTRODUCTION

Animal development is an extremely robust process that generally continues without major delays, regardless of perturbations and obstacles (Mestek Boukhibar and Barkoulas, 2016; Waddington, 1957). Once initiated, the sequence of developmental processes proceeds with great momentum, like a train on a railway, until an organism's mature form is reached. Yet, some animals are known for their exceptional ability to suspend abruptly their transition to adulthood for extended periods. For instance, the monarch butterfly (*Danaus plexippus*) typically grows from an egg to a fertile adult in 1 month during the summer; but if an individual emerges in the fall, the butterfly will pause its development at juvenile stages for 6-8 months as it migrates several thousand miles to warmer temperatures (Reppert and de Roode, 2018). Although it is known that insect species can undergo this type of growth delay (Tatar and Yin, 2001), the question of whether vertebrates are able to stay physically active, yet pause their organismic growth at juvenile stages without detrimental consequences is still open. Discovery of such a 'stay put' switch and delineation of the enabling mechanisms in vertebrate models may provide crucial insights into the regulatory control of growth and aging in humans.

Laboratory zebrafish exhibit a well-defined developmental trajectory consisting of four major stages: embryo, larva, juvenile and adult (Parichy et al., 2009). Despite minor differences in developmental timing between strains and rearing conditions, most individuals readily reach adulthood within 3 months under regular laboratory settings. Researchers routinely stage developing zebrafish according to visible external body features, such as incremental body lengths and heights, appearance of scales and fin rays, and development of pigment patterns (McMenamin et al., 2016; Parichy et al., 2009; Singleman and Holtzman, 2014). This ease of staging and the consistency of zebrafish development during post-embryonic stages has enabled researchers to model the mechanisms of allometric and ontogenetic growth, pigment pattern formation, and the onset of aging in a vertebrate animal (Chopra et al., 2019; Daane et al., 2018; Harris et al., 2020; Iovine et al., 2005; Kujawski et al., 2014; Li et al., 2020; McMenamin et al., 2014). Furthermore, it is worth noting that zebrafish are poikilothermic and thus amenable to temperature-sensitive screens (Chen and Poss, 2017). This key feature offers a unique opportunity to study essential genes that may have previously unidentified functions at the late developmental stages or during adult tissue regeneration.

From a forward genetic screen targeting key regulators of tissue regeneration (Chen et al., 2015), we identified a zebrafish mutant with temperature-sensitive defects in juvenile growth (*pan*). Long-term tracking of juvenile-staged individuals after return to the permissive temperature indicated that the *pan* phenotypes are fully reversible. No differences in anatomy or reproductive capability were apparent between the developmentally paused and released *pan* fish and their respective heterozygous siblings at the adult stage. Through positional cloning and classical complementation assays, we determined that *pan* phenotypes arise from an alteration in the gene encoding DEAD-Box Helicase 52 (*ddx52*). This mutation causes a splicing error that leads to a deletion of 25 amino acids near the C terminus of the protein. We further determined that, as a probable RNA helicase, Ddx52 activity is specifically required for maintaining the level of 47S precursor ribosomal RNA in live animals, thereby affecting bulk RNA transcription in proliferating tissues. Moreover, either genetic silencing of the *ddx52* ortholog in fruit flies or direct pharmacological inhibition of bulk RNA transcription in zebrafish and mice causes similar delays in growth. Thus, our study introduces a gene that is essential for post-embryonic growth in vertebrates and invertebrates, leading us

[1]Institute of Cellular and Organismic Biology, Academia Sinica, Taipei 11529, Taiwan. [2]Department of Cell Biology, Regeneration Next, Duke University Medical Center, Durham, NC 27710, USA.

*Author for correspondence (chcchen@gate.sinica.edu.tw)

T.-L.T., 0000-0003-1319-0141; Y.-T.W., 0000-0003-0184-2392; C.-Y.T., 0000-0003-3563-0187; Y.-T.K., 0000-0003-4887-3575; Y.-C.L., 0000-0002-7734-5619; H.-J.H., 0000-0001-7892-2310; K.D.P., 0000-0002-6743-5709; C.-H.C., 0000-0002-6825-1573

Handling Editor: Steve Wilson
Received 2 March 2021; Accepted 30 June 2021

Development (2021) 148, dev199578. doi:10.1242/dev.199578

to propose a conserved mechanism for modulating juvenile-to-adult transition trajectories.

RESULTS

Forward genetic screening identifies a temperature-sensitive mutant with a growth delay

As part of a systematic effort to identify key regulators of tissue regeneration, we performed a three-generation genetic screen for zebrafish mutants defective in tailfin regeneration (Chen et al., 2015). The screen was conducted on adult-stage fish under the restrictive temperature and aimed to isolate temperature-sensitive alleles for conditional studies (Johnson and Weston, 1995; Poss et al., 2002). Among the collection of regeneration-deficient mutants, we noticed that one, which we later named *pan* after Peter Pan, displayed impairments in both regeneration and growth. At 34°C, adult *pan* fish had greatly reduced fin growth at 7 days post-amputation (dpa) with complete penetrance (15/15; Fig. S1A). When kept at the permissive temperature (26°C), the *pan* regenerate length was normal or close to normal compared with heterozygous siblings (Fig. S1B), suggesting that *pan* is a bona fide temperature-sensitive (ts) allele. To determine whether *pan* affects specific phases of regeneration (i.e. wound healing, blastema formation or the outgrowth phase), we transferred animals from 26°C to 34°C at 0, 1, 2 or 4 dpa and examined the lengths of fin regenerates at 7 dpa. We found that transfer at any of the examined time points caused a significant reduction in regenerate length (Fig. S1C). Because the percentage reduction in fin length was less severe with later transfers (Fig. S1C), we concluded that *pan* activity is essential throughout all phases of regeneration. As tailfin regeneration is a complex morphogenetic process, we next examined whether *pan* is also required for simpler forms of repair, such as healing of an incision wound. As such, we made a straight cut in the inter-ray region of the tailfin tissue (Fig. S1D). This type of lesion only severs the inter-ray mesenchyme and epidermis, so the healing process takes just 2 days to complete in zebrafish (Chen et al., 2015). We found that both *pan* and *pan*/+ siblings exhibited complete healing of these wounds by 2 days post-incision (dpi) at 34°C (Fig. S1E). Thus, *pan* activity is dispensable for healing of a simple wound, which does not involve blastema formation. To determine whether *pan* is required for adult survival and tissue maintenance, we transferred fully developed animals at 3 months of age to 34°C for weekly monitoring. We found that both *pan* and *pan*/+ adults showed similar reductions in survival at the elevated temperature (survival was decreased by ∼30% after 21 days; Fig. S1F). Unlike previously reported *sde1* or other mutants (Chen et al., 2015; Wang et al., 2019; Wills et al., 2008b), we detected no signs of atrophy in tailfin tissues by 21 days post-treatment (dpt), except for a loss of pigment stripe (n=12/15; Fig. S1G). Thus, we conclude that the *pan* locus does not have an active role in maintaining the integrity of adult tissues.

To determine whether the *pan* locus is generally required for tissue morphogenesis, we examined its effects during juvenile growth. We transferred 4-week-old animals to 34°C for long-term monitoring (Fig. 1A). Of note, defining specific developmental stages of zebrafish based on age is often not accurate. Thus, we assessed the progression of organismic growth by both fish length and physical features, as previously described (McMenamin et al., 2016; Parichy et al., 2009; Singleman and Holtzman, 2014). Intriguingly, we found that growth of *pan* mutants was much reduced compared with the growth of heterozygous siblings. By 28 dpt, 8-week-old *pan* mutants were on average 27% shorter by standard length (SL) and 42% shorter in terms of height at anterior of anal fin (HAA) (Parichy et al., 2009) (Fig. 1B,C). In contrast, only 9% differences in SL could be detected between *pan* mutants and their heterozygous siblings when maintained at 26°C (Fig. S1H, I). To determine whether the mechanism underlying *pan*-induced defects in juvenile growth is specific to this mutant, we examined the growth phenotype of another regeneration mutant, *sde1*, which carries a ts allele for the gene encoding the extracellular matrix component *lamb1a* (Chen et al., 2015). In contrast to *pan*, we detected no delay in juvenile growth in *sde1* zebrafish, despite the expected evident signs of fin atrophy under the restrictive temperature (Chen et al., 2015) (Fig. 1B; bottom right). Thus, we conclude that the regulatory mechanisms governing tissue regeneration and juvenile growth are uncoupled in *sde1*, whereas juvenile growth is profoundly impacted by *pan* activity.

To determine whether *pan* is also required for late juvenile growth, we transferred 6-week-old animals to 34°C for 28 days. Again, only *pan*, but not *sde1*, produced a significant delay in late juvenile growth, according to SL and HAA measurements (Fig. 1D-F). The growth delay phenotype in *pan* also corresponded to delayed development of several physical adult characteristics, such as lack of adult barbels, immature pigment patterns, and absence or incomplete formation of calcified bone structures (Fig. 1G,H). Taken together, our data suggest that *pan* encodes a genetic determinant capable of attenuating growth at distinct juvenile stages. The effect of the *pan* mutation on growth at the restrictive temperature appears to be specific to the mutation, as we failed to detect similar phenotypes in other ts mutants within our collection (Chen et al., 2015; Wang et al., 2019; Whitehead et al., 2005).

Delayed growth phenotype in juvenile *pan* is fully reversible

Despite their reduced size and immature physical appearance, we detected no additional externally visible developmental anomalies or anatomical scaling defects (Chopra et al., 2019; Daane et al., 2018; Harris et al., 2020; Kujawski et al., 2014) in *pan* juveniles maintained at the restrictive temperature (Fig. 1). To identify long-term or possibly permanent defects in these individuals, we first inactivated *pan* for 28 days (from 4 to 8 weeks of age) and then monitored the growth-arrested fish at the permissive temperature for a 12-week period (Fig. 2A,B). Notably, we found that *pan* mutants readily resumed growth, eventually catching up with their heterozygous siblings by 20 weeks of age without notable phenotypic differences (Fig. 2B-D). To chart the growth trajectories of individual fish, we repeated the experiments and tracked each juvenile-staged fish over the entire recovery phase at the permissive temperature (one animal per 1.5-l tank; Fig. S2A,B). We found that restoration of *pan* activity accelerated the animal growth rate to a maximum of 2.4-fold over controls during a 4-week period (Fig. S2C). Thus, restoring *pan* activity is alone sufficient to jumpstart growth by raising the growth trajectory of an affected individual. To determine the maximum length of pause after which *pan* growth may resume, we inactivated *pan* for 56 consecutive days starting at 4 weeks of age. Remarkably, restoring *pan* activity in 3-month-old juveniles similarly boosted their growth, regardless of the long-term pause (Fig. S2D-F). Of note, key developmental features and growth remain coupled in *pan* mutants during the recovery phase, as determined by comparing the mutant phenotype with the normal table of postembryonic zebrafish development (Parichy et al., 2009) (SL and images of tailfin development and pigment pattern formation are shown in Fig. S3). To determine whether the growth-paused animals are able to acquire normal adult features after release, we performed two fertility assays on recovered *pan* individuals. We detected no significant differences in

Development (2021) 148, dev199578. doi:10.1242/dev.199578

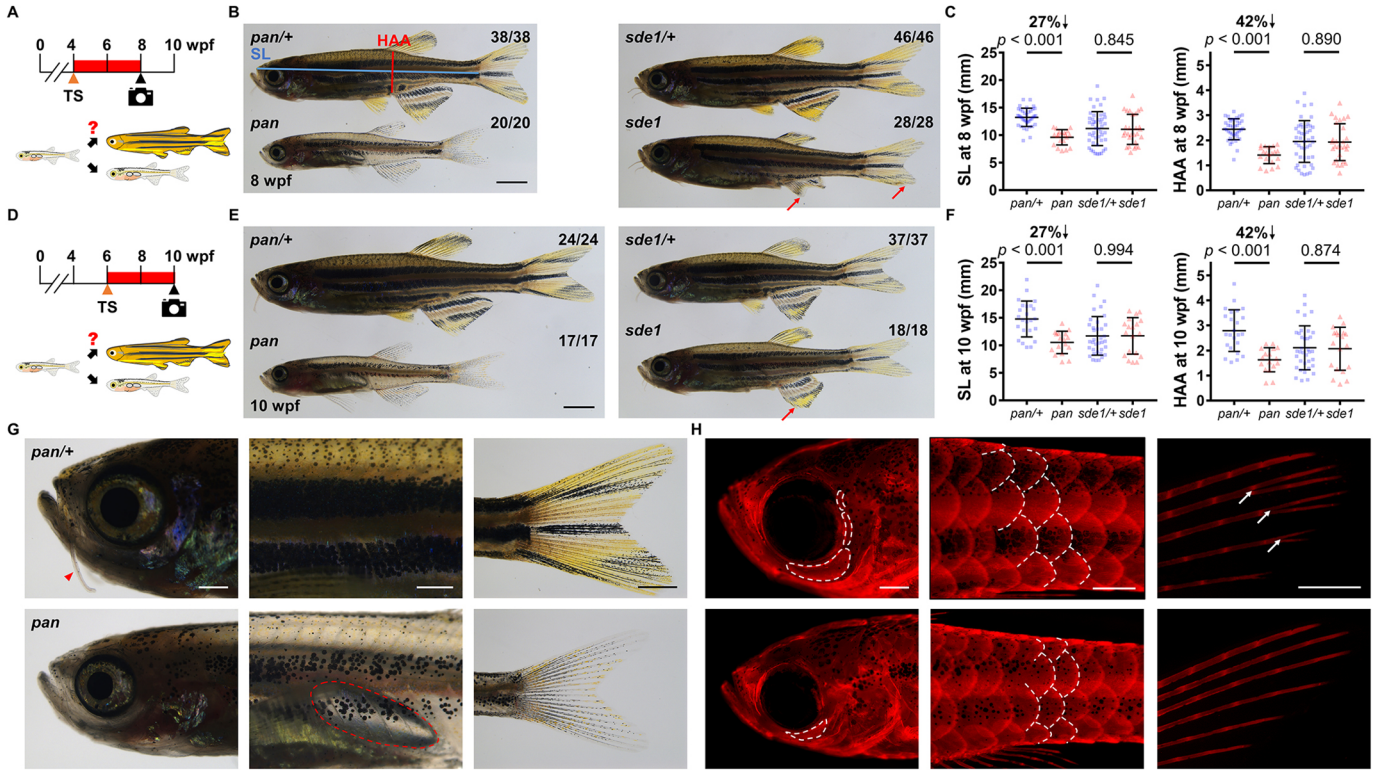

Fig. 1. Temperature-sensitive *pan* mutant has defects in juvenile growth. (A) Timeline of the temperature shift experiment during zebrafish development. TS, temperate shift; wpf, weeks post-fertilization. Red bar indicates time at 34°C. (B) Whole-mount images of *pan* and *pan*/+ individuals at 8 wpf (stitched) and *sde1* ts mutants, which were included as an experiment control for the effect of the restrictive temperature on regeneration mutants. Blue solid line indicates the measurement of standard length (SL). Red solid line indicates the measurement of height at anterior of anal fin (HAA). Red arrows point to severely degraded fin tissues in *sde1*. Scale bar: 2 mm. (C) Measurements of SL and HAA at 8 wpf (n=38 *pan*/+, 20 *pan*, 46 *sde1*/+, 28 *sde1*; mean±s.d.; two-tailed Student's *t*-test). (D) Timeline of a second temperature shift experiment during zebrafish development. (E) Whole-mount images of *pan* and *pan*/+ individuals at 10 wpf (stitched) and *sde1* ts mutants (experiment control for the effect of the restrictive temperature on regeneration mutants). Red arrow points to degraded fin tissues in *sde1*. Scale bar: 2 mm. (F) Measurements of SL and HAA at 10 wpf (n=24 *pan*/+, 17 *pan*, 37 *sde1*/+, 18 *sde1*; mean±s.d.; two-tailed Student's *t*-test). (G) Bright-field images of *pan*/+ and *pan* at 8 wpf after a 4-week incubation at 34°C. Red arrowhead points to the growth of adult barbels. Red dashed line indicates a swim bladder. Trunk areas and tailfins in *pan* fish remain mostly transparent, presumably as a result of defects in the generation of adult pigmentation patterns. Scale bars: 0.5 mm (left); 1 mm (middle and right). (H) Fluorescence images of *pan* at 8 wpf after a 4-week incubation at 34°C. Mature calcified bone structures were detected by Alizarin Red staining. *pan* lacks several craniofacial bones (left, dashed lines), displays defects in scale maturation (middle, dashed lines depict scale margins) and the tailfin has no bifurcation points (right, white arrows), a landmark feature in adult tailfin bony rays. Scale bars: 0.5 mm.

reproductive fitness, either in terms of male mating success rate or average number of viable progeny per mating event (Fig. 2E,F). Taken together, these results led us to conclude that *pan* may encode a switch-like regulator of growth with an activity that governs the juvenile-to-adult stage transition in zebrafish.

pan encodes *ddx52*, a putative RNA helicase

To identify the underlying mutation associated with the *pan* phenotype, we conducted whole-exome sequencing of genomic DNA from *pan*×*pan*/+ crosses (as described by Chen et al., 2015), followed by SNPtrack analysis of regions with high homozygosity (Leshchiner et al., 2012). This analysis yielded a single locus of 12.1 Mb on chromosome 21 (Fig. 3A). Phenotyping and genotyping of 757 adult animals from several mapping crosses revealed two closely linked single nucleotide polymorphisms (SNPs) in a 283 kb region (Fig. 3A). Next, cDNA sequencing of three candidate genes within this region (*heatr6*, *ddx52* and *traf4b*; Fig. 3A) led us to focus on two of the candidates: HEAT repeat containing 6 (*heatr6*) and DEAD (Asp-Glu-Ala-Asp)-box Helicase 52 (*ddx52*). Notably, both genes remain uncharacterized in vertebrate systems. Within *heatr6*, we detected two non-synonymous mutations, each causing distinct amino acid changes (M76L and G530S, shown in Fig. S4A). In contrast, we did not identify any non-synonymous mutations in *ddx52* exons. However, the cDNA displayed a splicing error in exons 13 and 14 that is expected to produce an in-frame deletion of 25 amino acids from the C-terminal domain of the putative protein (Fig. 3B,C). To determine which of these genes is responsible for the *pan* phenotype, we applied a CRISPR/Cas9-based approach (Talbot and Amacher, 2014) to generate stable deletion lines for complementation assays. We first established two deletion lines on a wild-type background for *heatr6* (*heatr6*$^{del\#1}$ and *heatr6*$^{del\#2}$ in Fig. S4B-D). After crossing F1 heterozygous animals with *pan*, we detected no regeneration deficits at the restrictive temperature in any adult *heart6*^{del}/*pan* individuals (n=0/19 for the *heatr6*$^{del\#1}$/*pan* and 0/35 for the *heatr6*$^{del\#2}$/*pan*; Fig. S4E). Thus, *heatr6* is not the functional gene in *pan*. Next, we generated a whole-gene deletion line of *ddx52* (Fig. 3C,D). In sharp contrast to the results with *heatr6*-deletion lines, we found that each of the *ddx52*^{del}/+×*pan*/*pan* crosses consistently generated high ratios of progeny with regeneration defects at the restrictive temperature. We determined that adult animals with and without the defects invariably matched their predicted genotype (n=23/23 for *pan*/+ and 12/12 for *ddx52*^{del}/*pan*; Fig. 3E). Thus, the *ddx52* null allele failed to complement *pan*.

Development (2021) 148, dev199578. doi:10.1242/dev.199578

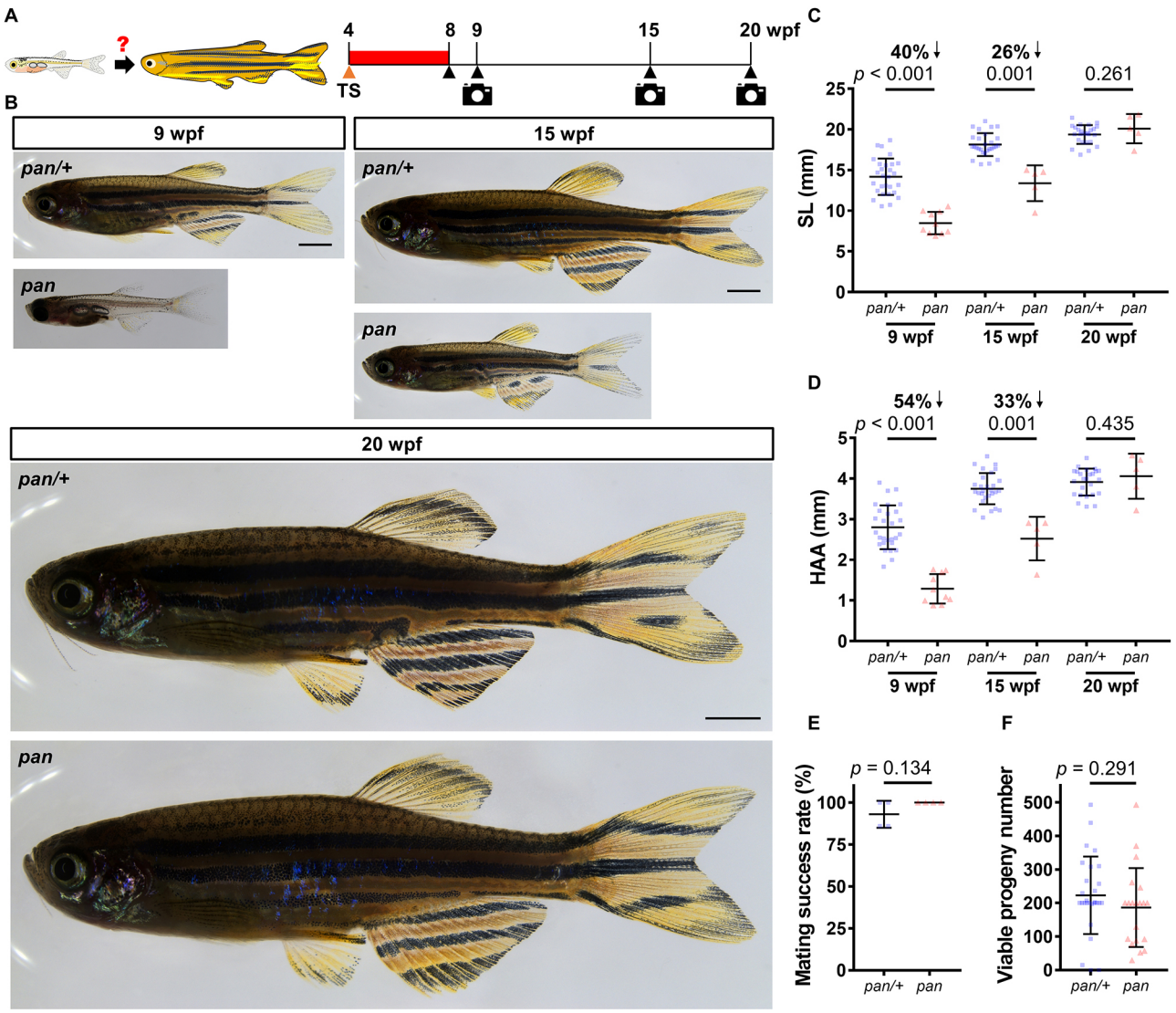

Fig. 2. Delayed growth phenotypes in *pan* are fully reversible. (A) Timeline of the temperature shift experiment during zebrafish development. TS, temperature shift; wpf, weeks post-fertilization. Red bar indicates the time at 34°C. (B) Whole-mount images of *pan* and *pan*/+ individuals after 4 weeks at 34°C (stitched). Following release from the restrictive temperature, images were captured at 9, 15 and 20 wpf. Scale bars: 2 mm. (C,D) Measurements of SL and HAA at 9, 15 and 20 wpf (9 wpf: *n*=28 *pan*/+, 10 *pan*; 15 wpf: 28 *pan*/+, 5 *pan*; 20 wpf: 25 *pan*/+, 5 *pan*; mean±s.d.; two-tailed Student's *t*-test). (E,F) Mating success rates and viable progeny numbers produced by each male *pan*/+ and *pan* individual (from four independent crosses). Consecutive crosses were set up with wild-type females at 2-week intervals (*n*=7 *pan*/+, 5 *pan*; mean±s.d.; two-tailed Student's *t*-test).

Based on high-resolution genetic and physical mapping, extensive Sanger sequencing of protein-coding exons, and complementation assays with three independently created stable deletion lines, we conclude that *ddx52* is the gene responsible for *pan* phenotypes.

To determine whether *ddx52* is required for early animal development, we examined progeny from several $ddx52^{del}$/+×$ddx52^{del}$/+ crosses. Consistent with Mendelian inheritance ratios, we found that about 25% of embryos displayed a shortened body length and a severe pericardial edema at 6 dpf (*n*=29/118 at 26°C; Fig. 3F), indicating that *ddx52* has an essential role in supporting early embryonic development. Taken together, these findings suggest that the truncated form of the Ddx52 protein likely acts as a hypomorph at the restrictive temperature to impair adult tailfin regeneration and juvenile growth.

Because *ddx52* activity appears to have a decisive role in regeneration and growth, we tested the idea that overexpression of *ddx52* may be sufficient to promote organismic growth. By creating a stable transgenic line *Tg(ubi:EGFP-2A-ddx52)* with constitutive high expression of *ddx52* in the whole body (19.3-fold; Fig. S5A-C), we determined that the body length is slightly increased at 8 dpf, but the difference becomes insignificant later in life compared with non-transgenic siblings (Fig. S5D). Thus, we speculated that *ddx52* may either function in a switch-like manner or it might act synergistically with yet-to-be-identified components in order to regulate regeneration and growth. It is equally possible that rapid growth during juvenile stages may have physiological limits that are difficult if not impossible to surpass.

Genetic targeting of the fruit fly *ddx52* ortholog prevents larva-to-adult transition

Because of its substantial influence on zebrafish growth, we hypothesized that the effect of *ddx52* on growth might extend to other distantly related animal species. To examine this idea, we tested the impact of *ddx52* silencing on the development of the fruit

Development (2021) 148, dev199578. doi:10.1242/dev.199578

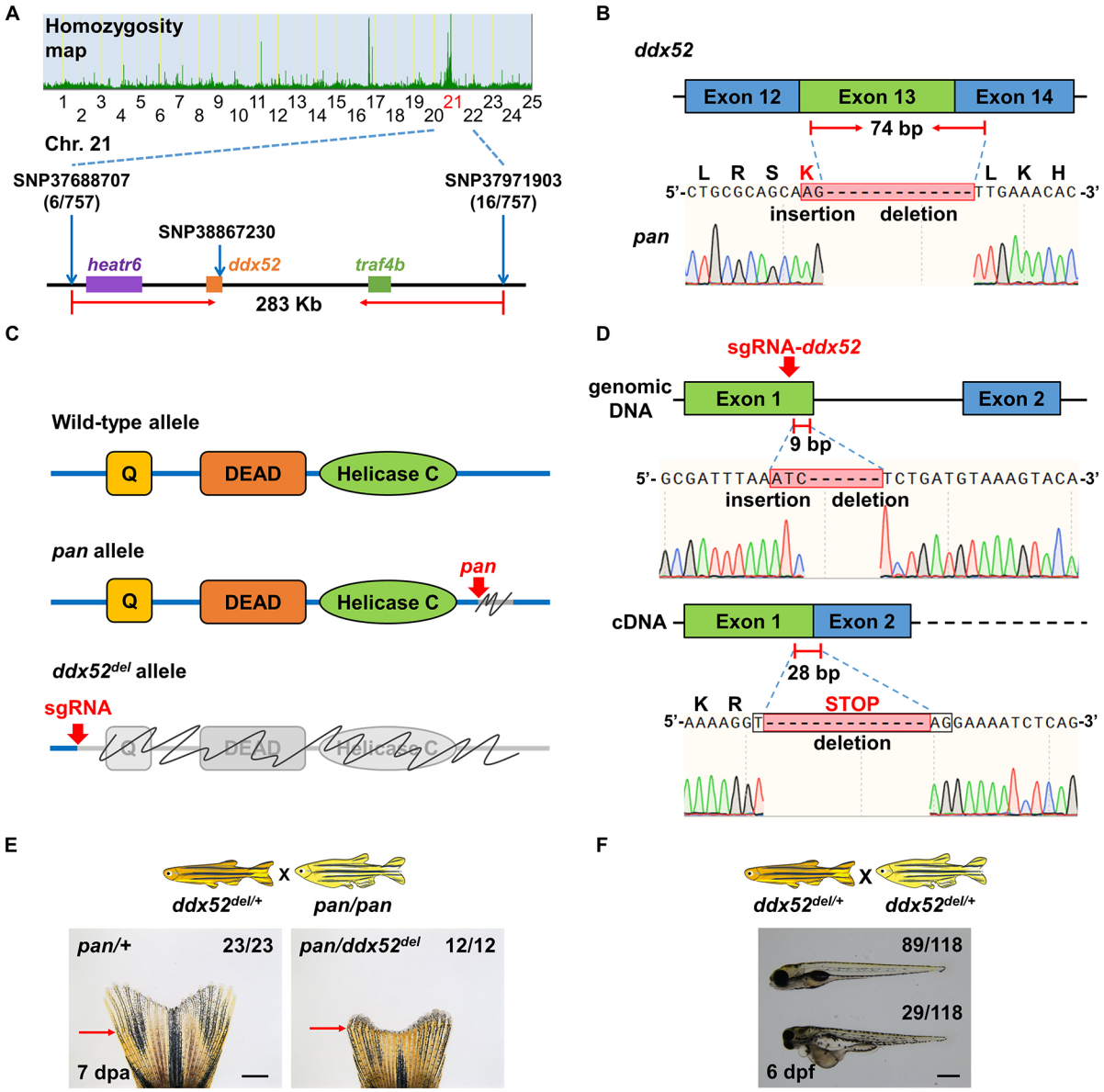

Fig. 3. *ddx52* is the *pan* gene. (A) High-resolution mapping of linked SNP markers in *pan*. Six and 16 recombinants were respectively identified for SNP37688707 and SNP37971903. SNP38867230 in *ddx52* exon 14 was used for detection of the *pan* allele. (B) Sanger sequencing readouts from *pan* cDNA. The *ddx52* sequence contains an in-frame indel that affects exons 13 and 14. (C) The three major structural domains of *ddx52*: Q motif, DEAD-box domain and helicase C domain. Gray color and scribble lines indicate regions that are affected in the *pan* allele and the $ddx52^{del}$ allele. (D) Illustration of and Sanger sequencing readouts depicting the sgRNA targeting site. The resulting $ddx52^{del}$ allele produces an out-of-frame indel that leads to an early stop codon in exon 2. (E) The $ddx52^{del}$ allele fails to complement the *pan* tailfin regeneration defect in adult animals. All adult animals with or without regeneration defects at the restrictive temperature had expected genotypes (n=23 *pan*/+, 12 *pan*/$ddx52^{del}$). Red arrows indicate the amputation plane. Scale bar: 1 mm. (F) Whole-mount images of $ddx52^{del}$×$ddx52^{del}$ embryos at 26°C. Approximately 25% of embryos had severe developmental defects at 6 days post-fertilization (dpf). Scale bar: 0.5 mm.

fly. Of note, the major protein domains encoded by *ddx52* orthologs are conserved (Fig. 4A,B), despite the fact that invertebrates and vertebrates diverged 700 million years ago (Kumar et al., 2017; Wray, 2015). The fly *ddx52* ortholog, *CG5589*, remains an uncharacterized gene (http://flybase.org/reports/FBgn0036754.html). To determine whether fly *ddx52* similarly affects developmental trajectories, we acquired two independently created RNAi knockdown transgenic lines (*UAS-CG5589*$^{RNAi\ BDSC}$ and *UAS-CG5589*$^{RNAi\ VDRC}$) to enable specific silencing of fly *ddx52*. To achieve global knockdown of *ddx52* mRNA expression, we crossed the RNAi lines with a driver line that has whole-tissue expression of GAL4 (Perkins et al., 2015). The combination effectively downregulated the fly *ddx52* level, as determined by RT-qPCR (decrease of 36% in *UAS-CG5589*$^{RNAi\ BDSC}$; Fig. 4C). As a control for non-specific effects of RNAi, we first determined that most animals (~97%) emerging from *act-GAL4*×*UAS-gfp*^{RNAi} crosses reach adult stages with genotypes occurring at expected ratios (n=231; Fig. 4D,E). In contrast, both *act-GAL4*×*UAS-CG5589*^{RNAi} crosses consistently generated high ratios of progeny that failed to grow into adult flies. By 25 days post-fertilization, up to 56% of the progeny remained stuck either at larval or pupal stages (n=331 and 284 from three independent crosses; Fig. 4D,E). We then genotyped flies that had achieved adulthood and found that none of the *act*>*UAS-CG5589*^{RNAi} double transgenic animals was present in the

Development (2021) 148, dev199578. doi:10.1242/dev.199578

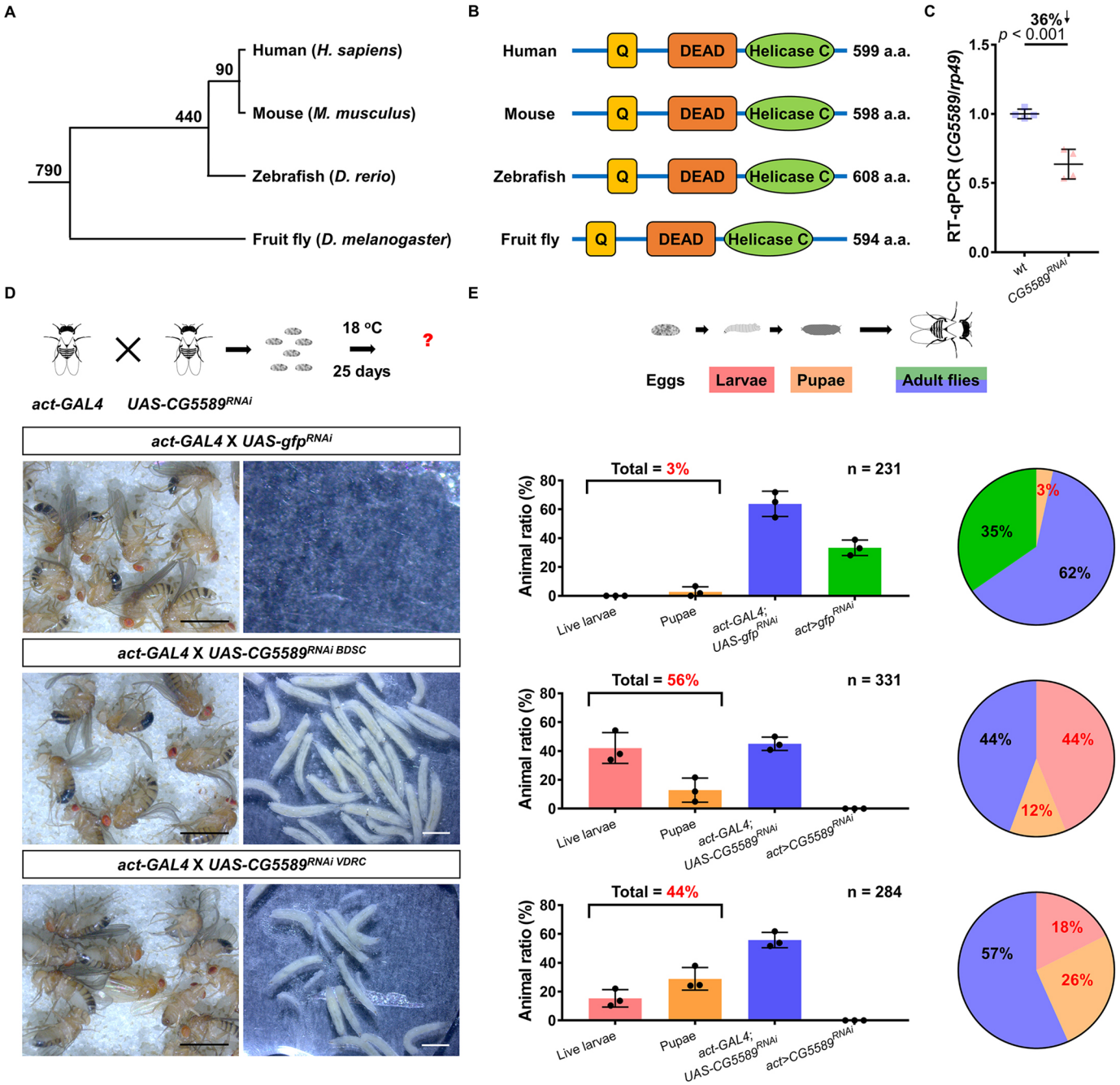

Fig. 4. Genetic silencing of the *ddx52* ortholog impedes development in the fruit fly. (A) A phylogenetic tree of vertebrate and invertebrate animals. Zebrafish, mice and fruit flies were examined in this study. The numbers next to each node indicate how many millions of years ago divergence took place. (B) The major structural domains of Ddx52 are conserved in different animal species. (C) RT-qPCR assay indicating the reduction of *ddx52* expression level in progeny from the *act-GAL4×UAS-CG5589*$^{RNAi\ BDSC}$ cross. qPCR results were normalized to *rp49* (n=4 per group; 40 larvae in each group; mean±s.e.m.; two-tailed Student's t-test). (D) Developmental phenotypes in the fruit fly upon genetic silencing of the *ddx52* ortholog, *CG5589*. In the *gfp*^{RNAi} control crosses, no live larvae were found after 25 days. In contrast, a large number of live larvae and pupae were detected in both of the *CG5589*^{RNAi} crosses. (E) Schematic shows the developmental trajectory of fruit flies. Bar charts show the percentages of animals detected at each developmental stage (mean ±s.d.). The numbers on the top right corner of each bar chart indicate the total numbers of animals examined in three independent crosses. Pie charts summarize the percentages of animals at each developmental stage.

adult pool (n=0/308; Fig. 4E). Thus, based on similar phenotypes from two independently created RNAi lines, we conclude that the previously uncharacterized fly *ddx52* is required for the larva-to-adult stage transition during development. These findings are consistent with the notion that *ddx52* has a profound and evolutionarily conserved role in supporting the progression of organismic growth.

Ddx52 maintains transcription of 47S precursor ribosomal RNA and bulk RNA

Despite a lack of research on *ddx52* in animal models, studies on the yeast homolog and other DEAD-box RNA helicase family members suggest it may have potential roles in ribosome biogenesis, ribosomal RNA (rRNA) synthesis and RNA editing (Khoshnevis et al., 2016; Linder and Jankowsky, 2011; Song et al.,

Development (2021) 148, dev199578. doi:10.1242/dev.199578

1995; Venema et al., 1997). Specifically, mammalian Ddx52, along with other DEAD-box containing RNA helicases, affects the quantity of 47S precursor rRNA (pre-rRNA) in a cell culture system (Zhang et al., 2011). As the first product of the rRNA synthesis cascade, 47S pre-rRNA has a short lifespan and is rapidly processed into the mature rRNAs (i.e. 18S, 28S and 5.8S) once transcribed (Fig. 5A). Thus, one can examine the quantity of 47S pre-rRNA as a readout for the rates of its transcription and the overall rRNA synthesis (Cui and Tseng, 2004; Zhang et al., 2011). To determine whether *ddx52* similarly regulates 47S pre-rRNA in live animals, we transiently inactivated Ddx52 activity in *pan* mutants and detected the removal of the 5′-external transcribed space (5′ETS) on 47S pre-rRNA by RT-qPCR (Bouffard et al., 2018) (Fig. 5A,B). Intriguingly, we found that a brief 6-h inactivation of Ddx52 in regenerating tailfin tissues markedly reduced the level of 47S pre-rRNA by 44% in the 4 dpa blastema (Fig. 5C). In contrast, the treatment had little or no effect on the 18S rRNA level, which presumably is much more stable *in vivo* (Fig. 5D). Notably, the Ddx52 influence on 47S pre-rRNA is likely to be specific and direct, as the release of the inactivation

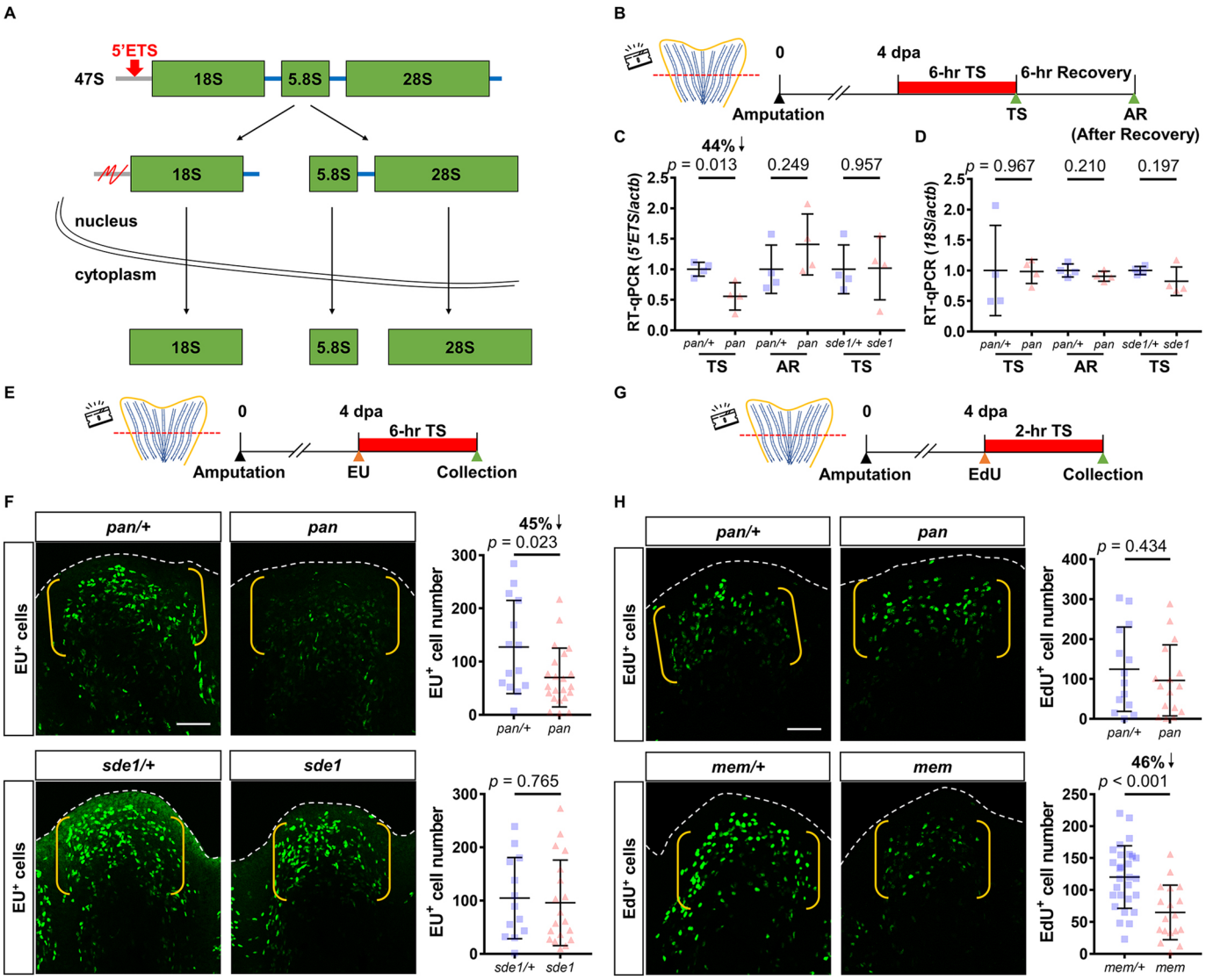

Fig. 5. Ddx52 maintains 47S pre-rRNA and bulk RNA transcriptions in proliferating tissues. (A) Illustration depicting the processing of ribosomal RNAs. Once transcribed, the 47S pre-rRNA is immediately processed into 18S, 5.8S and 28S rRNAs. Red arrow points to the 5′-external transcribed space (5′ETS), the level of which often serves as a readout for the quantity of 47S pre-rRNA. (B) Timeline of the temperature shift experiment during tailfin regeneration. AR, after recovery at 26°C; dpa, days post-amputation; TS, temperature shift. Red bar indicates time at 34°C. (C) RT-qPCR assay indicating a marked reduction in the 5′ETS level after a 6-h incubation at 34°C. qPCR results were normalized to *actb* (n=4 per group; mean±s.e.m.; two-tailed Student's t-test). (D) RT-qPCR assay indicating no change in the 18S level after a 6-h incubation at 34°C. qPCR results were normalized to *actb* (n=4 per group; mean±s.e.m.; two-tailed Student's t-test). (E) Timeline of the temperature shift and EU assay during tailfin regeneration. Orange arrowhead marks the EU injection time. TS, temperature shift. Red bar indicates time at 34°C. (F) Whole-mount EU staining of *pan* and *sde1* tailfin regenerates at 4 dpa after a 6-h incubation at 34°C. White dashed lines outline the distal margin of the fin tissue. Yellow brackets mark the blastema compartment. Scale bar: 50 µm. Graphs show quantification of EU$^+$ cells in the lateral 2nd bony ray (n=24 *pan*/+, 22 *pan*; 13 *sde1*/+, 19 *sde1*; mean±s.d.; two-tailed Student's t-test). (G) Timeline of the temperature shift and EdU assay during tailfin regeneration. Orange arrowhead marks the EdU injection. Red bar indicates time at 34°C. (H) Whole-mount EdU staining of *pan* and *mem* tailfin regenerates at 4 dpa after a 2-h incubation at 34°C. White dashed lines outline the distal margin of the fin tissue. Yellow brackets mark the blastema compartment. Scale bar: 50 µm. Graphs show quantification of EdU$^+$ cells in the lateral 2nd bony ray (n=14 *pan*/+, 16 *pan*; 28 *mem*/+, 18 *mem*; mean±s.d.; two-tailed Student's t-test).

Development (2021) 148, dev199578. doi:10.1242/dev.199578

rapidly restored the pre-rRNA expression in less than 6 h (Fig. 5B,C).

Because up to 60% of total cellular RNA synthesis is devoted to rRNA transcription (Warner, 1999), we further hypothesized that Ddx52-mediated, transient blocking of the pre-rRNA synthesis should have a drastic impact on the level of bulk RNA transcription. To test this idea, we established a 5-ethynyl uridine (EU) incorporation assay (Jao and Salic, 2008) in regenerating tailfin tissues to detect dynamic changes in total RNA synthesis. We found that abruptly switching-off Ddx52 activity had an immediate influence on the number of EU-positive cells in the 4 dpa blastema (decrease of 45%; Fig. 5E,F). This impact is not generalizable to other ts mutants, as transient inactivation of *lamb1a* activity in *sde1* mutants had no measurable effects on the level of 47S pre-rRNA or the number of EU-positive cells (Fig. 5C,F). As additional controls for specificity of the effect, we determined that transient inactivation of Ddx52 for 6 h had no effect on the levels of *shha* and *lef1*, i.e. specific messenger RNA species that are key for tissue regeneration (Fig. S6A,B); nor did it affect the level of DNA synthesis in proliferating tissues compared with *mem* mutants carrying a ts allele of a DNA polymerase subunit (Wang et al., 2019) (Fig. 5G,H). Taken together, these experiments using direct and temporal modulation of Ddx52 activity in intact and live animals led us to conclude that Ddx52 is constantly required for the synthesis of 47S pre-rRNA; thus, it maintains bulk RNA transcription in real time.

We then determined the spatiotemporal expression pattern of *ddx52* in regenerating tailfin tissues by RT-qPCR and RNA *in situ* hybridization assays. We found that *ddx52* is rapidly induced by 6 h post amputation (hpa) and remains upregulated until at least 48 hpa in the mesenchymal compartment (Fig. S6C,D). Intriguingly, the induction of *ddx52* transcripts upon wounding appears to be a common occurrence in many regenerative tissues, including tailfin, heart, liver, muscle, lateral line and different glial cells (http://www.zfregeneration.org/) (Nieto-Arellano and Sánchez-Iranzo, 2018). In our system of tailfin amputation, we determined that the induction of *ddx52* is not affected by injury level, wound healing perturbations, or Fgf and Wnt/β-Catenin signaling pathways (Fig. S6E-H). Thus, although we were unable to identify a specific wound signal responsible for *ddx52* activation, stimulation of *ddx52* function during regeneration seems to be a conserved phenomenon across distinct tissue types and organs.

Pharmacological suppression of bulk RNA transcription reversibly pauses regeneration and growth in zebrafish

Our finding that the main mechanism by which *ddx52* affects regeneration and growth is through suppression of 47S pre-rRNA synthesis and subsequent reduction in protein translation (Fig. S6I,J) was predictable based on the expected functions of the gene. Yet, we were intrigued by the full reversibility of the growth pause caused by the acute suppression of RNA transcription. To test whether direct, pharmacological suppression of bulk RNA transcription could reproduce *pan* phenotypes during regeneration and growth, we treated wild-type animals with actinomycin D (Act D), a potent inhibitor of RNA transcription and common cancer chemotherapeutic agent (Bensaude, 2011; Liu et al., 2016). Of note, Act D may have multiple mechanisms of action; however, it is most effective at blocking the activity of RNA polymerase I, which only transcribes 47S pre-rRNA (Bensaude, 2011; Russell and Zomerdijk, 2006). To determine the effective dose of Act D for suppressing bulk RNA transcription, we performed the EU assay in regenerating tailfin tissues. Notably, we found that a single dose of 100 µg/ml Act D markedly reduced the number of EU-positive cells (decrease of 93%; Fig. 6A,B), mimicking the effect of *pan* on bulk RNA transcription (Fig. 5F). To test whether Act D treatment can reversibly pause tissue growth during regeneration, we intraperitoneally injected adult zebrafish upon tailfin amputation. As expected, the Act D-treated animals had a smaller regenerate at 4 dpa compared with vehicle-treated animals (Fig. 6C,D). Intriguingly, the effect of Act D on regenerates was transient and fully reversible, as we detected no morphological or size differences at 21 dpa when regenerates were compared with respective pre-injury fin structures (15/15; Fig. 6D-F). In contrast, when we treated animals with hydroxyurea (HU), a potent inhibitor of DNA replication, the treatment similarly reduced fin regenerate size at 4 dpa, yet many regenerates (~93%) failed to restore the pre-injury shape and size by 21 dpa (Fig. 6D-F). These HU-induced changes in fin regenerates are likely to be permanent, as previously shown (Wang et al., 2019). To examine further the reversible effect of Act D on organismic growth, we intraperitoneally injected 11-week-old wild-type juveniles. As expected, the Act D-treated animals had significantly reduced growth at 21 dpt compared with vehicle-treated siblings (decrease of 8.4% in SL and 11% in HAA; Fig. 6G-J). Yet, consistent with the regeneration and *pan* phenotypes, the effect of Act D on growth was transient and fully reversible; we detected no morphological or length differences between vehicle- and Act D-treated fish at 49 dpt (Fig. 6H-J). Taken together, these results support the notion that direct targeting of 47S pre-rRNA or bulk RNA transcriptions may allow non-detrimental, reversible pausing of adult regeneration and juvenile growth. We further speculate that the RNA-based mechanism is at least somewhat specific, as targeting DNA replication machineries similarly affects tissue growth but fails to reproduce the reversible effect.

Transient Act D treatment reversibly pauses growth in developing mice

These findings led us to investigate whether the growth pausing mechanism may be generalizable to higher vertebrates, such as mammals. Therefore, we examined next the effect of Act D on a commonly used laboratory mouse strain (C57BL/6). We administered a series of 0.25 mg/kg doses to 4-week-old juvenile mice. As expected, the treatment drastically impaired growth of the animals at 11 dpt, as determined by a marked reduction in body length and tail length (Fig. 7A-C). Of note, we measured 'tail length' as an unambiguous readout reflecting the overall development of the vertebral column (Lee et al., 2017). To determine whether the treatment does indeed cause a developmental pause, we performed a high-resolution micro-CT scan of the growth-paused mice and their respective vehicle-treated siblings at 11 dpt. A significant reduction in skull length and size was observed (Fig. 7D-F), supportive of a bona fide developmental arrest. Intriguingly, yet consistent with our findings in *pan* and Act D-treated zebrafish, we found that the affected individuals readily resumed growth and development upon release from treatment, eventually catching up with the vehicle-treated animals by 46 dpt in a repeated experiment. We detected no significant differences in skull length, skull size, tail length, daily food intake, body length or body weight between vehicle- and Act D-treated animals at 46 dpt (Fig. 7D-K). To determine whether Act D may cause any minor developmental defects that may be missed in a gross examination, we further examined the micro-CT scan captured at 46 dpt. Notably, despite the fact that there was no marked difference in the femur length, the end-point scans revealed a slight yet statistically significant reduction in the tibia length of Act

Development (2021) 148, dev199578. doi:10.1242/dev.199578

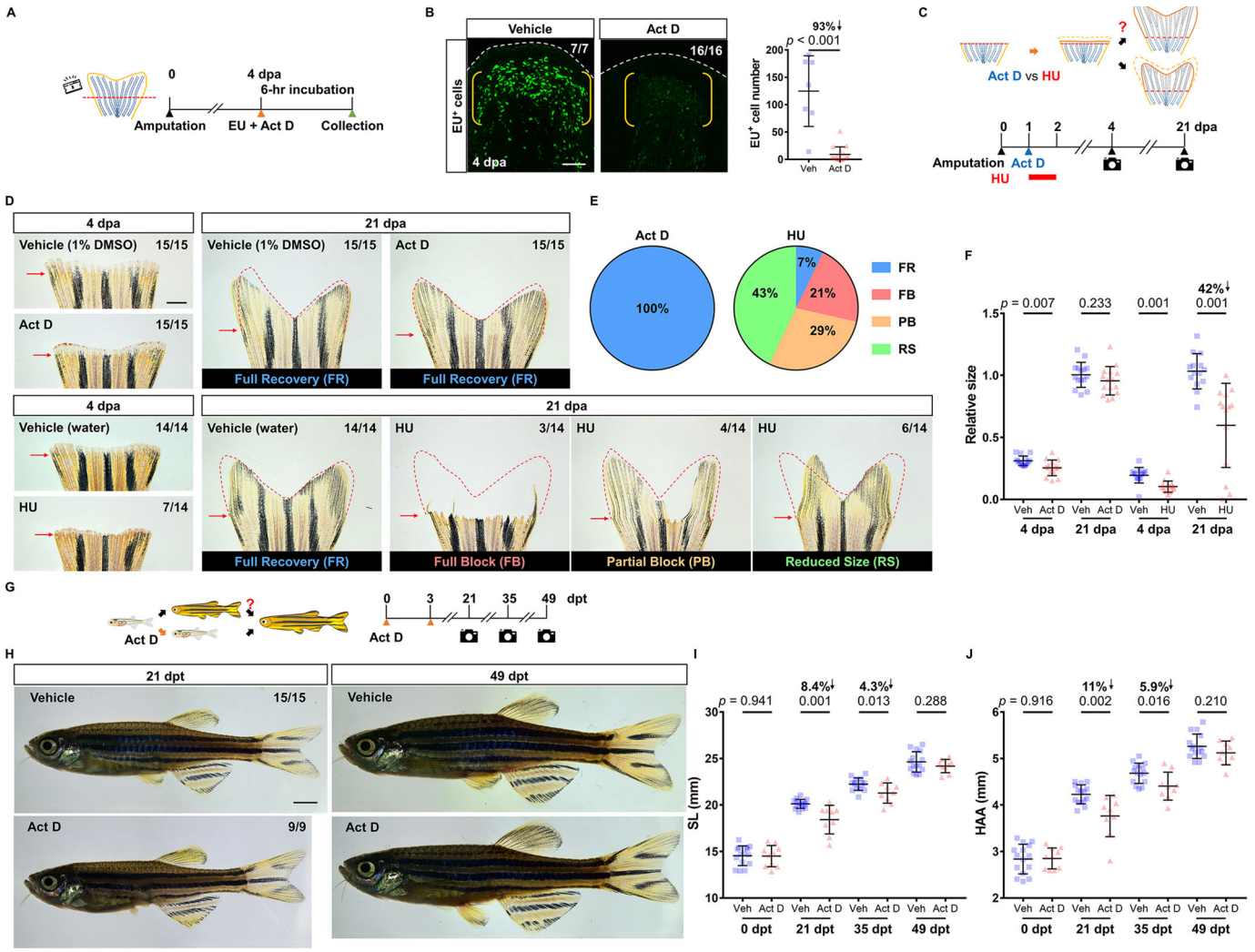

Fig. 6. Pharmacological inhibition of bulk RNA transcription reversibly pauses regeneration and growth in zebrafish. (A) Timeline of actinomycin D (Act D) treatment and EU assay during tailfin regeneration. Orange arrowhead marks the EU and Act D injection time. Green arrowhead marks the collection time. (B) Whole-mount EU staining of the wild-type tailfin regenerates at 4 dpa after a 6-h treatment of Act D. White dashed lines outline the distal margin of the fin tissue. Yellow brackets mark the blastema compartment. Scale bar: 50 µm. Graph shows quantification of EU$^+$ cells in the lateral 2nd bony ray (n=7 vehicle, 16 Act D; mean±s.d.; Mann–Whitney U test). (C) Timeline of Act D and HU treatment during tailfin regeneration. In the Act D group, individuals at 1 dpa were intraperitoneally injected with either vehicle or Act D, as indicated by a blue arrowhead. In the HU group, individuals at 1 dpa were incubated in either vehicle or HU for 24 h, as indicated by a red bar. Fin regenerates were imaged at 4 and 21 dpa. (D) Whole-mount images of the Act D/HU-treated WT fin regenerates at 4 and 21 dpa. Red arrows indicate amputation plane. Red dashed lines depict respective fin region prior to the amputation to facilitate visual comparison. Scale bar: 1 mm. (E) Pie charts summarizing proportions of fin regenerate phenotypes at 21 dpa. Left: All of the regenerates in the Act D group (15/15) fully recovered. Right: Fin regenerates in the HU group displayed high variation. Only 7% of the animals (1/14) fully recovered. FB, full block; FR, full recovery; PB, partial block; RS, reduced size. (F) Quantification of the relative fin regenerate size. Data from each individual were normalized to their original fin sizes (n=15 vehicle, 15 Act D; 14 vehicle, 14 HU; mean±s.d.; two-tailed Student's t-test). (G) Timeline of Act D treatment in juvenile zebrafish. Individuals at 11 weeks of age were intraperitoneally injected twice with either vehicle or Act D, as indicated by orange arrowheads. Images were captured at 21, 35 and 49 days after the first treatment (dpt). (H) Whole-mount images of the vehicle- and Act D-treated zebrafish at 21 and 49 dpt (stitched). Scale bar: 2 mm. (I,J) Measurements of SL and HAA at 0, 21, 35 and 49 dpt (n=15 vehicle, 9 Act D; mean±s.d.; two-tailed Student's t-test).

D-treated animals at 46 dpt (decreased by 3.4%; Fig. 7L-N). Taken together, the similar findings from zebrafish and mouse models suggest that short-term, direct suppression of 47S pre-RNA and/or bulk RNA transcription by Act D treatment has a profound but largely reversible impact on juvenile growth across different vertebrate species.

DISCUSSION

Because it encodes a putative RNA helicase, the effect of *ddx52* on growth may be mediated in part through its direct influence on specific mRNA transcripts. Despite our observation of similar growth phenotypes upon pharmacological inhibition of bulk RNA transcription, it is possible that Ddx52 has important, specific mRNA targets or that it regulates aspects of rRNA metabolism other than the synthesis of pre-rRNA. Consistent with this notion, Bennett et al. (2018) showed that genetic deficiency of *ddx27*, another DEAD-box RNA helicase, similarly affects pre-rRNA synthesis as well as the translation of a specific subset of mRNA transcripts in zebrafish embryos. Notably, the *ddx27* phenotypes appear to be tissue specific, predominantly affecting skeletal muscle growth and regeneration. This study and ours highlight the complexity faced when pinpointing the exact *in vivo* targets of an individual RNA helicase. Thus, we do not expect that *ddx52* is a master regulator of animal development with an exclusive role on 47S pre-rRNA

Development (2021) 148, dev199578. doi:10.1242/dev.199578

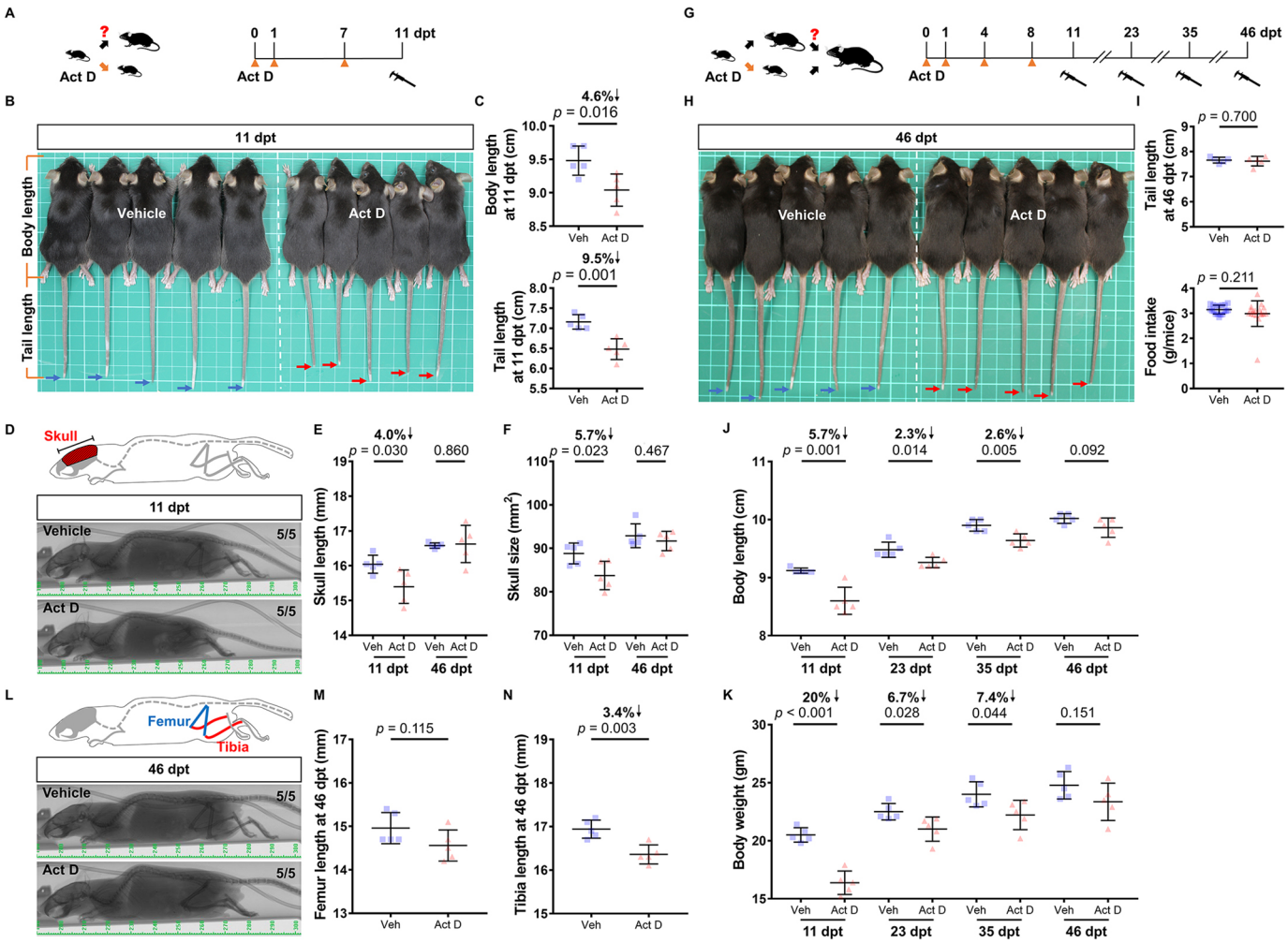

Fig. 7. Transient inhibition of RNA transcription reversibly pauses growth in mice. (A) Timeline of Act D treatment in juvenile mice. Mice at 4 weeks of age were intraperitoneally injected with either vehicle or Act D three times, as indicated by orange arrowheads. Caliper indicates measurement. (B) Bright-field image of the mice at 11 dpt. Blue and red arrows point to mouse tail-tips. White squares are 1 cm on each side. (C) Measurements of body length and tail length at 11 dpt (n=5 vehicle, 5 Act D; mean±s.d.; two-tailed Student's t-test). (D) Top: Illustration of mouse skull. Measured regions are highlighted in red. Bottom: Micro-CT scans of vehicle- and Act D-treated mice at 11 dpt. Major unit: 1 cm. (E,F) Measurements of skull length and skull size at 11 and 46 dpt (n=5 vehicle, 5 Act D; mean±s.d.; two-tailed Student's t-test). (G) Timeline of Act D treatment in juvenile mice in a repeated experiment. Mice at 4 weeks old were injected intraperitoneally with either vehicle or Act D four times, as indicated by the orange arrowheads. (H) Bright-field image of the mice at 46 dpt. Blue and red arrows point to mouse tail-tips. White squares are 1 cm on each side. (I) Measurements of tail length at 46 dpt and average daily food intake (4 to 46 dpt) (n=5 vehicle, 5 Act D from a total of 15 measurements; mean±s.d.; two-tailed Student's t-test for tail length analysis; Mann–Whitney U-test for average daily food intake). (J,K) Measurements of body length and body weight at 11, 23, 35 and 46 dpt (n=5 vehicle, 5 Act D; mean±s.d.; two-tailed Student's t-test). (L) Top: Illustration of relevant mouse bone structures. Femur (blue) and tibia (red) bone lengths were compared. Bottom: Micro-CT scans of vehicle- and Act D-treated mice at 46 dpt. Major unit: 1 cm. (M,N) Measurements of femur and tibia bone lengths at 46 dpt (n=5 vehicle, 5 Act D; mean±s.d.; two-tailed Student's t-test).

synthesis. Rather, our findings suggest that intricate control of RNA transcription or metabolism may offer a unique opportunity to safely suspend post-embryonic growth for an extended period.

Besides specific genetic factors, the growth of zebrafish may be affected by certain rearing conditions, including nutrient supply, oxygen levels, temperature, and aquarium density (Kamei et al., 2018; Kimmel et al., 1995; Wills et al., 2008a). Upon release from adverse, low-growth conditions, affected individuals may enter a catch-up period of rapid growth until the adult form is reached. Thus, it will be interesting to determine whether *ddx52* or other DEAD-box RNA helicase family members (Zhang et al., 2011) might influence growth progression under known low-growth conditions, acting as a downstream effector of the environmental influences on animal growth and development. Of note, when manipulating Ddx52 activity, the progression of growth and development remained coupled in *pan* mutants (Fig. S3). This key feature is distinct from growth mutants that are defective in hormonal signaling, such as the *gh1* and *duox* mutants (Chopra et al., 2019; McMenamin et al., 2013). In both of those mutants, growth is severely inhibited, but the animals still display many developmental characteristics of adults.

When juvenile monarch butterflies suspend their transition to a fully adult stage, their lifespan is quadrupled with respect to conspecifics that do not delay the transition (Herman and Tatar, 2001). Even though we detected no morphological or functional anomalies in released adult *pan* fish (Fig. 2), it is not known whether a 2-month delay in the developmental course will have any lasting impact on the animal's lifespan (lab-raised zebrafish have a generation time of 2-3 months, but may live up to 4 years). Moreover, we found that prolonged exposure to the restrictive

Development (2021) 148, dev199578. doi:10.1242/dev.199578

temperature negatively affects the survival of treated animals, regardless of their genotype (Fig. S1F). Thus, we have limited our use of the *pan* mutant to examining long-term growth suspension. Nevertheless, it will be interesting to determine whether intermittent inactivation of Ddx52 or RNA transcription may further lengthen juvenile stages, thereby altering the subsequent adult life-course trajectory of affected individuals.

In this work, we describe one scenario in which animal growth may be suspended or delayed at juvenile stages. The *pan* mutants are generally as physically active as juvenile-staged individuals at the restrictive temperature. Despite some similarities, the animal state studied here is distinct from the state of 'embryonic diapause' (Hand et al., 2016; Hussein et al., 2020; Renfree and Fenelon, 2017). As a survival strategy triggered by harsh environmental conditions, such as temperature, drought, or scarcity of food, diapause in embryonic animals involves physical and metabolic inactivity, and the animals may remain completely dormant for extremely long periods of time. The mechanisms of diapause and diapause-like states are currently being examined, and an intriguing study from Romney et al. (2018) has demonstrated that direct perturbation of vitamin D signaling can induce a diapause-like state in embryos of killifish and zebrafish. By incubating fertilized embryos in dafadine A, an inhibitor of vitamin D3 synthesis, the robust development of zebrafish embryos could be suspended for 2 days (Romney et al., 2018). In another recent study from Hu et al. (2020), the authors identified a specific chromatin regulator, CBX7, that is essential for maintaining the level of metabolism and the diapause state in killifish. Additionally, inhibition of mTOR, the mammalian target of rapamycin, has been reported to induce a diapause-like state in pre-implanted mouse embryos and cultured blastocysts (Bulut-Karslioglu et al., 2016; Hussein et al., 2020). Intriguingly, the underlying pausing mechanism is tightly associated with a robust, global suppression of RNA transcription (Bulut-Karslioglu et al., 2016), reminiscent of the effects we saw with Ddx52 inactivation or Act D treatment. Thus, it will be interesting to determine whether the mechanism we described here – an acute, direct suppression of RNA transcription or pre-rRNA synthesis – affect developmental timing in different contexts.

In summary, we provide a proof of concept that the activity of a single gene can dictate post-embryonic growth of the whole animal in a vertebrate model. Our findings regarding *ddx52* and its potent effect on RNA transcription highlight an evolutionarily conserved mechanism that could be hijacked to achieve robust, yet reversible control of ontogenetic growth in complex animals.

MATERIALS AND METHODS

Experimental model and subject details

Animal experiments were approved by and performed in accordance with guidelines provided by the Institutional Animal Care and Utilization Committee (IACUC) at Academia Sinica. For zebrafish, the Ekkwill strain of zebrafish was maintained at four to six individuals per liter at 26°C. Animals at 4 weeks to 12 months of age were used for experiments. Of note, for experiments with juvenile animals, gender identity was not determined owing to lack of external sex characteristics. *pan* zebrafish are also referred to as pd335 (*ddx52*^{pd335}). Deletion lines for *heatr6* and *ddx52* are referred to as as58 (*heatr6*$^{del\#1}$), as59 (*heatr6*$^{del\#2}$) and as60 (*ddx52*^{del}). The *ddx52* overexpression line is referred to as as64, *Tg(ubi:EGFP-2A-ddx52)*. *lamb1a* (*sde1*), *pola2* (*mem*) and *fgf20a* mutants (*dob*) were described previously (Chen et al., 2015; Wang et al., 2019; Whitehead et al., 2005). For fruit flies, *Actin* (*act*)-*GAL4/CyO* (B#4414), *UAS-gfp*^{RNAi} (B#41552), *UAS-CG5589*$^{RNAi\ BDSC}$ (B#32334) and *UAS-CG5589*$^{RNAi\ VDRC}$ (V#44322) were obtained from Bloomington *Drosophila* Stock Center (BDSC) or Vienna *Drosophila* Resource Center (VDRC). Fly stocks were maintained at 22-25°C on standard medium. To mimic the effect of a hypomorphic allele, offspring of GAL4 and RNAi were raised at 18°C, and the numbers of each genotype among adult flies, pupae and larvae were counted manually. For mice, 4-week-old C57BL/6JNarl mice were obtained from the National Laboratory Animal Center, Taiwan. The mice were maintained in a specific pathogen-free room with controlled temperature and moisture, and a 14-h light/10-h dark cycle.

Amputation, *pan* inactivation, and microscopy

For tailfin amputation, 50% of the tailfin was removed by a single cut with a razor blade. Animals were anesthetized in fish water containing tricaine (0.2 mg/ml) until fully sedated. Fin regenerate length was measured along the 2nd lateral bony ray from the dorsal side. For tailfin incision injuries, cuts were made under a dissecting microscope with a razor blade to the inter-ray region; the incision length was approximately two-thirds of the proximodistal length of the tailfin. To inactivate *ddx52* activity in *pan* zebrafish, mutants were shifted to a constant temperature at 34°C for the time period indicated in each figure. Of note, when shifted to 34°C at 5 wpf, *pan*/+ and *pan* had similar survival rates at 9 wpf (wild type, 80%; *pan*/+, 73%; *pan*, 73%; n=30 each). Whole-animal and tailfin images were captured using a Leica M205 stereomicroscope with a high-resolution camera (Leica DFC7000T). Large-field, whole-animal images were stitched together using Image Composite Editor (Microsoft Research). Histology images were captured with either a compound microscope (Leica DM750) or a laser scanning confocal microscope (Leica SP8; HC PL APO 20×/0.75 CS2, WD 0.62 mm).

Genetic mapping and positional cloning

Mutagenesis, regeneration mutant screens, initial genetic and physical mapping were described previously (Chen et al., 2015). Primer sequences for detecting SNP37688707, SNP37971903 and SNP38867230 (shown in Fig. 3A) are listed in Table S1. SNP38867230 was used to detect the *ddx52*^{pan} allele in high resolution melt (HRM) assays.

Generation of *ddx-52* overexpression transgenic line

Tg(ubi:EGFP-2A-ddx52)^{as64} was generated with a transgenic construct consisting of a 3.5 kb *ubi* promoter (Mosimann et al., 2011), the EGFP-2A, and *ddx52* cDNA sequences. The construct was flanked with I-SceI sites to facilitate transgenesis.

Generation of stable deletion lines by CRISPR/Cas9

sgRNAs targeting the *heatr6* and *ddx52* genomic regions were designed using CHOPCHOP (http://chopchop.cbu.uib.no/) (Labun et al., 2016; Montague et al., 2014). Primer sequences used to generate sgRNA templates and detect deletions are listed in Table S1. sgRNAs were synthesized from PCR fragment templates using the MEGAshortscript T7 Transcription Kit (Invitrogen, AM1354), as described (Talbot and Amacher, 2014). sgRNAs (200-300 ng/µl in 2 µl each) targeting the *heatr6* or *ddx52* genomic regions were co-injected with 2 µl Cas9 protein (1 µg/µl; PNA Bio, CP01-200) into one-cell-stage zebrafish embryos. Genetic lesions were detected by PCR using the primers listed in Table S1. Positive F0 clutches were raised to adulthood and outcrossed with wild-type animals. To establish stable deletion lines, F1 animals were raised to adulthood for genotyping. Complementation assays were conducted using heterozygous F1 animals with respective deletions.

Fertility assays

To determine the mating success rate, adult male animals were assessed four times at 2-week intervals by pairing with wild-type females. The ratio was determined as (number of spawned males/total number of examined males)×100%. Spawned eggs from each mating pair were collected, counted and recorded for viability. The number of successfully developed embryos was recorded as the viable progeny number. Results from four independent crosses were pooled for comparison.

EU and EdU assays

For EU incorporation assays, 10 µl EU solution (Invitrogen, E10345; 10 mM in 50% DMSO in PBS) was intraperitoneally injected into each

Development (2021) 148, dev199578. doi:10.1242/dev.199578

adult zebrafish 6 h prior to collection of tailfin regenerates. Tissues were fixed with 4% paraformaldehyde (Sigma-Aldrich, P6148) in PBS at 4°C overnight and processed as described, with some modifications (Jao and Salic, 2008). After fixation, fin tissues were washed twice with PBST (PBS with 0.1% Tween-20) for 5 min each time and transferred into methanol. Fin tissues were washed in methanol twice, for 10 min each time, and transferred into PBST. Next, tissues were incubated in freshly prepared Click-iT staining solution (1 mM $CuSO_4$, 50 mM ascorbic acid, 10 µM fluorescent azide and 100 mM Tris buffer, pH 8.0) for 1 h at room temperature before washing with PBST four times, 5 min each. Finally, fin tissues were mounted in Fluoromount G for imaging by confocal microscopy (Leica SP8; HC PL APO 20×/0.75 SC2, WD 0.62 mm).

5-Ethynyl-2′-deoxyuridine (EdU) incorporation assays were conducted as described (Wang et al., 2019). Briefly, 10 µl EdU solution (Molecular Probes, A10044; 10 mM in 50% DMSO in PBS) was injected intraperitoneally 1 h prior to collection of tailfin regenerates. Fin tissues were fixed in Carnoy's fixative (30% chloroform and 10% acetic acid in ethanol) for 3 h at room temperature, followed by methanol washes, 10 min each, and transfer into PBST. Next, tissues were incubated in freshly prepared Click-iT staining solution for 30 min at room temperature before four PBST washes of 5 min each. Fin tissues were mounted in Fluoromount G for imaging by confocal microscopy.

Treatment of signaling modulators, gadolinium, actinomycin D and hydroxyurea

To manipulate the Wnt signaling pathway after a 50% tailfin amputation, zebrafish were incubated in fish water with 12 µM IWR-1 (Sigma-Aldrich, I0161-5G), 100 nM BIO (Sigma-Aldrich, B1686-5MG) or 0.02% DMSO for 6 h. Tailfin tissues were then collected for RNA extraction. To perturb the wound healing response after a 50% tailfin amputation, zebrafish were incubated with 100 µM Gd^{3+} (Sigma-Aldrich, G7532-5G) for 2 h. Animals were rinsed and kept in fish water for another 4 h before collecting tailfin tissues for RNA extraction.

To block bulk RNA transcription in zebrafish, Act D dissolved in 1% DMSO/PBS was intraperitoneally injected into adults (10 µl each; 100 µg/ml); a lower dose was injected into 11-week-old juveniles (5 µl each; 10 µg/ml) after anesthesia with tricaine (0.2 mg/ml) for 3-5 min. To block bulk RNA transcription in juvenile mice, Act D in 1% DMSO/PBS was intraperitoneally injected at a dosage of 0.25 mg/kg. To block DNA synthesis, live zebrafish were incubated in 20 mM hydroxyurea (Sigma-Aldrich, H8627) from 24 to 48 hpa as described (Wang et al., 2019).

In vivo Alizarin Red S staining

Live zebrafish were incubated in 500 ml 0.01% ARS (Sigma-Aldrich, A5533) for 15 min at room temperature before rinsing for three times in fish water, 5 min each, according to a previously described protocol (Bensimon-Brito et al., 2016). Images of stained animals were acquired using a Leica M250 FA fluorescence stereomicroscope.

RNA *in situ* hybridization (ISH), RT-qPCR and HRM assays

ISH, RT-qPCR and HRM assays were performed as described (Wang et al., 2019). To generate digoxigenin-labeled probes, *shha* (1.2 kb), *lef1* (1.1 kb) and *ddx52* (0.2 kb) cDNA sequences were cloned from zebrafish cDNA and then inserted into pCR2.1-TOPO vectors as synthesis templates (see Table S1). Primers used in RT-qPCR and HRM assays are listed in Table S1.

Histological assays

For whole-mount immunostaining of tenascin C, tailfin tissues were collected and fixed in Carnoy's fixative for 3 h at room temperature, followed by methanol washes for 10 min each and then transfer to PBST. Next, tissues were incubated in freshly prepared blocking buffer [10% heat inactivated newborn calf serum (Gibco, 26010066), 2% horse serum (Gibco, 16050130) and 0.1% DMSO in PBST] at 37°C for 30 min. Tissues were then incubated with antibodies against tenascin C (US Biological, T2550-23; 1:250) in blocking buffer without horse serum at 37°C for 4 h. After incubating with the secondary antibody (Invitrogen, A110037; 1:500) at 37°C for 30 min, tissues were then washed four times in PBST, 5 min each, and mounted in Fluoromount G for imaging by laser confocal microscopy (Leica SP8; HC PL APO 20×/0.75 SC2, WD 0.62 mm).

Body length, tail length and micro-CT measurements in mice

Body length was measured from the tip of the nose to the base of the tail; tail length was measured from the base of the tail to the tail tip. For micro-CT examinations, mice were euthanized before conducting two-dimensional imaging of whole mice and hind limbs (Skyscan 1076 system; Bruker) in the Taiwan Mouse Clinic, Academia Sinica. The scanning parameters were set as follows: image pixel size 9 µm, X-ray voltage 50 kV, X-ray current 140 µA, filter A1 0.5 mm, exposure 3300 ms, rotation step 0.8°, frame averaging 2, tomographic rotation 180°.

Quantification and statistical analysis

Statistical analyses were performed using GraphPad Prism 7. Data points from groups that had sufficient n number were tested for Gaussian distribution using the D'Agostino–Pearson test. If the data points were normally distributed, we used two-tailed Student's unpaired t-test to determine P-values. If the data were not normally distributed, we used non-parametric two-tailed Mann–Whitney U-test for comparison. Statistical parameters (i.e. exact n values, what n represents, s.e.m., s.d., etc.) are listed in the figure legends.

Acknowledgements

We thank Hsiao-Yuh Roan, Chung-Han Wang, and the Taiwan Zebrafish Core Facility (TZCAS; MOST 108-2319-B-400-002) for zebrafish care; Stephan Schneider, Jr-Kai Yu and Yi-Hsien Su for discussions; Chen laboratory members for comments on the manuscript; Marcus J. Calkins for English editing and comments.

Competing interests

The authors declare no competing or financial interests.

Author contributions

Conceptualization: K.D.P., C.-H.C.; Methodology: T.-L.T., Y.-T.W., C.-Y.T., Y.-T.K., Y.-C.L., H.-J.H., K.D.P., C.-H.C.; Validation: T.-L.T., Y.-T.W., C.-Y.T., Y.-T.K., Y.-C.L., H.-J.H., C.-H.C.; Formal analysis: T.-L.T., Y.-T.W., C.-Y.T., Y.-T.K., Y.-C.L., H.-J.H., C.-H.C.; Investigation: T.-L.T., Y.-T.W., C.-Y.T., Y.-T.K., Y.-C.L., H.-J.H., C.-H.C.; Resources: K.D.P., C.-H.C.; Data curation: T.-L.T., Y.-T.W., Y.-C.L., H.-J.H., C.-H.C.; Writing - original draft: C.-H.C.; Writing - review & editing: T.-L.T., Y.-T.W., K.D.P.; Visualization: T.-L.T., Y.-T.W., C.-Y.T., Y.-T.K., C.-H.C.; Supervision: Y.-C.L., H.-J.H., C.-H.C.; Project administration: C.-H.C.; Funding acquisition: Y.-C.L., H.-J.H., K.D.P., C.-H.C.

Funding

We acknowledge intramural funding from the Institute of Cellular and Organismic Biology, Academia Sinica (C.-H.C., H.-J.H., and Y.-C.L.); grant support from Academia Sinica (AS-CDA-109-L03 to C.-H.C.), the Ministry of Science and Technology, Taiwan (MOST 106-2628-B-001-001-MY4 to C.-H.C.; MOST 108-2320-B-001-022 to Y.-C.L.) and the National Institutes of Health (R01 GM074057 and R01 AR076342 to K.D.P.). Deposited in PMC for release after 12 months.

Peer review history

The peer review history is available online at https://journals.biologists.com/dev/article-lookup/doi/10.1242/dev.199578.

References

Bennett, A. H., O'Donohue, M.-F., Gundry, S. R., Chan, A. T., Widrick, J., Draper, I., Chakraborty, A., Zhou, Y., Zon, L. I., Gleizes, P.-E. et al. (2018). RNA helicase, DDX27 regulates skeletal muscle growth and regeneration by modulation of translational processes. *PLoS Genet.* **14**, e1007226. doi:10.1371/journal.pgen.1007226

Bensaude, O. (2011). Inhibiting eukaryotic transcription: Which compound to choose? How to evaluate its activity? *Transcription* **2**, 103-108. doi:10.4161/trns.2.3.16172

Bensimon-Brito, A., Cardeira, J., Dionísio, G., Huysseune, A., Cancela, M. L. and Witten, P. E. (2016). Revisiting in vivo staining with alizarin red S–a valuable approach to analyse zebrafish skeletal mineralization during development and regeneration. *BMC Dev. Biol.* **16**, 2. doi:10.1186/s12861-016-0102-4

Bouffard, S., Dambroise, E., Brombin, A., Lempereur, S., Hatin, I., Simion, M., Corre, R., Bourrat, F., Joly, J.-S. and Jamen, F. (2018). Fibrillarin is essential for S-phase progression and neuronal differentiation in zebrafish dorsal midbrain and retina. *Dev. Biol.* **437**, 1-16. doi:10.1016/j.ydbio.2018.02.006

Bulut-Karslioglu, A., Biechele, S., Jin, H., Macrae, T. A., Hejna, M., Gertsenstein, M., Song, J. S. and Ramalho-Santos, M. (2016). Inhibition of mTOR induces a paused pluripotent state. *Nature* **540**, 119-123. doi:10.1038/nature20578

Chen, C.-H. and Poss, K. D. (2017). Regeneration Genetics. *Annu. Rev. Genet.* **51**, 63-82. doi:10.1146/annurev-genet-120116-024554

Chen, C.-H., Merriman, A. F., Savage, J., Willer, J., Wahlig, T., Katsanis, N., Yin, V. P. and Poss, K. D. (2015). Transient laminin beta 1a induction defines the wound epidermis during Zebrafish fin regeneration. *PLoS Genet.* **11**, e1005437. doi:10.1371/journal.pgen.1005437

Chopra, K., Ishibashi, S. and Amaya, E. (2019). Zebrafish duox mutations provide a model for human congenital hypothyroidism. *Biol. Open* **8**, bio037655. doi:10.1242/bio.037655

Cui, C. and Tseng, H. (2004). Estimation of ribosomal RNA transcription rate in situ. *BioTechniques* **36**, 134-138. doi:10.2144/04361RR04

Daane, J. M., Lanni, J., Rothenberg, I., Seebohm, G., Higdon, C. W., Johnson, S. L. and Harris, M. P. (2018). Bioelectric-calcineurin signaling module regulates allometric growth and size of the zebrafish fin. *Sci. Rep.* **8**, 10391. doi:10.1038/s41598-018-28450-6

Hand, S. C., Denlinger, D. L., Podrabsky, J. E. and Roy, R. (2016). Mechanisms of animal diapause: recent developments from nematodes, crustaceans, insects, and fish. *Am. J. Physiol. Regul. Integr. Comp. Physiol.* **310**, R1193-R1211. doi:10.1152/ajpregu.00250.2015

Harris, M. P., Daane, J. M. and Lanni, J. (2020). Through veiled mirrors: fish fins giving insight into size regulation. *Wiley Interdiscip. Rev. Dev. Biol.* **10**, e381. doi:10.1002/wdev.381

Herman, W. S. and Tatar, M. (2001). Juvenile hormone regulation of longevity in the migratory monarch butterfly. *Proc. Biol. Sci.* **268**, 2509-2514. doi:10.1098/rspb.2001.1765

Hu, C.-K., Wang, W., Brind'Amour, J., Singh, P. P., Reeves, G. A., Lorincz, M. C., Alvarado, A. S. and Brunet, A. (2020). Vertebrate diapause preserves organisms long term through Polycomb complex members. *Science* **367**, 870-874. doi:10.1126/science.aaw2601

Hussein, A. M., Wang, Y., Mathieu, J., Margaretha, L., Song, C., Jones, D. C., Cavanaugh, C., Miklas, J. W., Mahen, E., Showalter, M. R. et al. (2020). Metabolic control over mTOR-dependent diapause-like state. *Dev. Cell* **52**, 236-250.e237. doi:10.1016/j.devcel.2019.12.018

Iovine, M. K., Higgins, E. P., Hindes, A., Coblitz, B. and Johnson, S. L. (2005). Mutations in connexin43 (GJA1) perturb bone growth in zebrafish fins. *Dev. Biol.* **278**, 208-219. doi:10.1016/j.ydbio.2004.11.005

Jao, C. Y. and Salic, A. (2008). Exploring RNA transcription and turnover in vivo by using click chemistry. *Proc. Natl. Acad. Sci. USA* **105**, 15779-15784. doi:10.1073/pnas.0808480105

Johnson, S. L. and Weston, J. A. (1995). Temperature-sensitive mutations that cause stage-specific defects in Zebrafish fin regeneration. *Genetics* **141**, 1583-1595. doi:10.1093/genetics/141.4.1583

Kamei, H., Yoneyama, Y., Hakuno, F., Sawada, R., Shimizu, T., Duan, C. and Takahashi, S.-I. (2018). Catch-up growth in zebrafish embryo requires neural crest cells sustained by Irs1 signaling. *Endocrinology* **159**, 1547-1560. doi:10.1210/en.2017-00847

Khoshnevis, S., Askenasy, I., Johnson, M. C., Dattolo, M. D., Young-Erdos, C. L., Stroupe, M. E. and Karbstein, K. (2016). The DEAD-box protein Rok1 orchestrates 40S and 60S ribosome assembly by promoting the release of Rrp5 from Pre-40S ribosomes to allow for 60S maturation. *PLoS Biol.* **14**, e1002480. doi:10.1371/journal.pbio.1002480

Kimmel, C. B., Ballard, W. W., Kimmel, S. R., Ullmann, B. and Schilling, T. F. (1995). Stages of embryonic development of the zebrafish. *Dev. Dyn.* **203**, 253-310. doi:10.1002/aja.1002030302

Kujawski, S., Lin, W., Kitte, F., Börmel, M., Fuchs, S., Arulmozhivarman, G., Vogt, S., Theil, D., Zhang, Y. and Antos, C. L. (2014). Calcineurin regulates coordinated outgrowth of zebrafish regenerating fins. *Dev. Cell* **28**, 573-587. doi:10.1016/j.devcel.2014.01.019

Kumar, S., Stecher, G., Suleski, M. and Hedges, S. B. (2017). TimeTree: a resource for timelines, timetrees, and divergence times. *Mol. Biol. Evol.* **34**, 1812-1819. doi:10.1093/molbev/msx116

Labun, K., Montague, T. G., Gagnon, J. A., Thyme, S. B. and Valen, E. (2016). CHOPCHOP v2: a web tool for the next generation of CRISPR genome engineering. *Nucleic Acids Res.* **44**, W272-W276. doi:10.1093/nar/gkw398

Lee, Y.-C., Song, I.-W., Pai, Y.-J., Chen, S.-D. and Chen, Y.-T. (2017). Knock-in human FGFR3 achondroplasia mutation as a mouse model for human skeletal dysplasia. *Sci. Rep.* **7**, 43220. doi:10.1038/srep43220

Leshchiner, I., Alexa, K., Kelsey, P., Adzhubei, I., Austin-Tse, C. A., Cooney, J. D., Anderson, H., King, M. J., Stottmann, R. W., Garnaas, M. K. et al. (2012). Mutation mapping and identification by whole-genome sequencing. *Genome Res.* **22**, 1541-1548. doi:10.1101/gr.135541.111

Li, C., Barton, C., Henke, K., Daane, J., Treaster, S., Caetano-Lopes, J., Tanguay, R. L. and Harris, M. P. (2020). celsr1a is essential for tissue homeostasis and onset of aging phenotypes in the zebrafish. *eLife* **9**, e50523. doi:10.7554/eLife.50523

Linder, P. and Jankowsky, E. (2011). From unwinding to clamping - the DEAD box RNA helicase family. *Nat. Rev. Mol. Cell Biol.* **12**, 505-516. doi:10.1038/nrm3154

Liu, X. F., Xiang, L., Zhou, Q., Carralot, J.-P., Prunotto, M., Niederfellner, G. and Pastan, I. (2016). Actinomycin D enhances killing of cancer cells by immunotoxin RG7787 through activation of the extrinsic pathway of apoptosis. *Proc. Natl. Acad. Sci. USA* **113**, 10666-10671. doi:10.1073/pnas.1611481113

McMenamin, S. K., Minchin, J. E. N., Gordon, T. N., Rawls, J. F. and Parichy, D. M. (2013). Dwarfism and increased adiposity in the gh1 mutant zebrafish vizzini. *Endocrinology* **154**, 1476-1487. doi:10.1210/en.2012-1734

McMenamin, S. K., Bain, E. J., McCann, A. E., Patterson, L. B., Eom, D. S., Waller, Z. P., Hamill, J. C., Kuhlman, J. A., Eisen, J. S. and Parichy, D. M. (2014). Thyroid hormone-dependent adult pigment cell lineage and pattern in zebrafish. *Science* **345**, 1358-1361. doi:10.1126/science.1256251

McMenamin, S. K., Chandless, M. N. and Parichy, D. M. (2016). Working with zebrafish at postembryonic stages. *Methods Cell Biol.* **134**, 587-607. doi:10.1016/bs.mcb.2015.12.001

Mestek Boukhibar, L. and Barkoulas, M. (2016). The developmental genetics of biological robustness. *Ann Bot* **117**, 699-707. doi:10.1093/aob/mcv128

Montague, T. G., Cruz, J. M., Gagnon, J. A., Church, G. M. and Valen, E. (2014). CHOPCHOP: a CRISPR/Cas9 and TALEN web tool for genome editing. *Nucleic Acids Res.* **42**, W401-W407. doi:10.1093/nar/gku410

Mosimann, C., Kaufman, C. K., Li, P., Pugach, E. K., Tamplin, O. J. and Zon, L. I. (2011). Ubiquitous transgene expression and Cre-based recombination driven by the ubiquitin promoter in zebrafish. *Development* **138**, 169-177. doi:10.1242/dev.059345

Nieto-Arellano, R. and Sánchez-Iranzo, H. (2018). zfRegeneration: a database for gene expression profiling during regeneration. *Bioinformatics* **35**, 703-705. doi:10.1093/bioinformatics/bty659

Parichy, D. M., Elizondo, M. R., Mills, M. G., Gordon, T. N. and Engeszer, R. E. (2009). Normal table of postembryonic zebrafish development: staging by externally visible anatomy of the living fish. *Dev. Dyn.* **238**, 2975-3015. doi:10.1002/dvdy.22113

Perkins, L. A., Holderbaum, L., Tao, R., Hu, Y., Sopko, R., McCall, K., Yang-Zhou, D., Flockhart, I., Binari, R., Shim, H.-S. et al. (2015). The transgenic RNAi Project at Harvard Medical School: resources and validation. *Genetics* **201**, 843-852. doi:10.1534/genetics.115.180208

Poss, K. D., Nechiporuk, A., Hillam, A. M., Johnson, S. L. and Keating, M. T. (2002). Mps1 defines a proximal blastemal proliferative compartment essential for zebrafish fin regeneration. *Development* **129**, 5141-5149. doi:10.1242/dev.129.22.5141

Renfree, M. B. and Fenelon, J. C. (2017). The enigma of embryonic diapause. *Development* **144**, 3199-3210. doi:10.1242/dev.148213

Reppert, S. M. and de Roode, J. C. (2018). Demystifying Monarch butterfly migration. *Curr. Biol.* **28**, R1009-R1022. doi:10.1016/j.cub.2018.02.067

Romney, A. L. T., Davis, E. M., Corona, M. M., Wagner, J. T. and Podrabsky, J. E. (2018). Temperature-dependent vitamin D signaling regulates developmental trajectory associated with diapause in an annual killifish. *Proc. Natl. Acad. Sci. USA* **115**, 12763-12768. doi:10.1073/pnas.1804590115

Russell, J. and Zomerdijk, J. C. B. M. (2006). The RNA polymerase I transcription machinery. *Biochem. Soc. Symp.* **73**, 203-216. doi:10.1042/bss0730203

Singleman, C. and Holtzman, N. G. (2014). Growth and maturation in the zebrafish, Danio rerio: a staging tool for teaching and research. *Zebrafish* **11**, 396-406. doi:10.1089/zeb.2014.0976

Song, Y., Kim, S. and Kim, J. (1995). ROK1, a high-copy-number plasmid suppressor of kem1, encodes a putative ATP-dependent RNA helicase in Saccharomyces cerevisiae. *Gene* **166**, 151-154. doi:10.1016/0378-1119(96)80010-2

Talbot, J. C. and Amacher, S. L. (2014). A streamlined CRISPR pipeline to reliably generate zebrafish frameshifting alleles. *Zebrafish* **11**, 583-585. doi:10.1089/zeb.2014.1047

Tatar, M. and Yin, C.-M. (2001). Slow aging during insect reproductive diapause: why butterflies, grasshoppers and flies are like worms. *Exp. Gerontol.* **36**, 723-738. doi:10.1016/S0531-5565(00)00238-2

Venema, J., Bousquet-Antonelli, C., Gelugne, J. P., Caizergues-Ferrer, M. and Tollervey, D. (1997). Rok1p is a putative RNA helicase required for rRNA processing. *Mol. Cell. Biol.* **17**, 3398-3407. doi:10.1128/MCB.17.6.3398

Waddington, C. (1957). *The Strategy of the Genes*. George Allen & Unwin.

Wang, Y.-T., Tseng, T.-L., Kuo, Y.-C., Yu, J.-K., Su, Y.-H., Poss, K. D. and Chen, C.-H. (2019). Genetic reprogramming of positional memory in a regenerating appendage. *Curr. Biol.* **29**, 4193-4207.e4194. doi:10.1016/j.cub.2019.10.038

Warner, J. R. (1999). The economics of ribosome biosynthesis in yeast. *Trends Biochem. Sci.* **24**, 437-440. doi:10.1016/S0968-0004(99)01460-7

Whitehead, G. G., Makino, S., Lien, C. L. and Keating, M. T. (2005). fgf20 is essential for initiating zebrafish fin regeneration. *Science* **310**, 1957-1960. doi:10.1126/science.1117637

Wills, A. A., Holdway, J. E., Major, R. J. and Poss, K. D. (2008a). Regulated addition of new myocardial and epicardial cells fosters homeostatic cardiac growth and maintenance in adult zebrafish. *Development* **135**, 183-192. doi:10.1242/dev.010363

Wills, A. A., Kidd, A. R., III, Lepilina, A. and Poss, K. D. (2008b). Fgfs control homeostatic regeneration in adult zebrafish fins. *Development* **135**, 3063-3070. doi:10.1242/dev.024588

Wray, G. A. (2015). Molecular clocks and the early evolution of metazoan nervous systems. *Philos. Trans. R. Soc. Lond. B Biol. Sci.* **370**. doi:10.1098/rstb.2015.0046

Zhang, Y., Forys, J. T., Miceli, A. P., Gwinn, A. S. and Weber, J. D. (2011). Identification of DHX33 as a mediator of rRNA synthesis and cell growth. *Mol. Cell. Biol.* **31**, 4676-4691. doi:10.1128/MCB.05832-11